AIP Advances

Enhancement and quenching of photoluminescence from silicon quantum dots by silver nanoparticles in a totally integrated configuration

A. Benami, A. López-Suárez, L. Rodríguez-Fernández, A. Crespo-Sosa, J. C. Cheang-Wong, J. A. Reyes-Esqueda, and A. Oliver

Citation: AIP Advances **2**, 012193 (2012); doi: 10.1063/1.3701696
View online: http://dx.doi.org/10.1063/1.3701696
View Table of Contents: http://scitation.aip.org/content/aip/journal/adva/2/1?ver=pdfcov
Published by the AIP Publishing

Enhancement and quenching of photoluminescence from silicon quantum dots by silver nanoparticles in a totally integrated configuration

A. Benami,[1,2,a] A. López-Suárez,[2,a] L. Rodríguez-Fernández,[2] A. Crespo-Sosa,[2] J. C. Cheang-Wong,[2] J. A. Reyes-Esqueda,[2] and A. Oliver[2]
[1]*Département de Physique FSTE, Université Moulay Ismail, Boutalamine B.P. 509, Errachidia, Morocco*
[2]*Instituto de Física, Universidad Nacional Autónoma de México, México D.F. 04510, México*

(Received 23 May 2011; accepted 14 March 2012; published online 29 March 2012)

In this study, Si QDs were formed inside silica matrix by implantation and annealing. Subsequent implantations with Ag^{+2} ions at different energies were performed in order to vary the distance between the previously formed Si QDs and newly aggregated Ag NPs. The coupling between them was observed through the PL energy and intensity from Si QDs. A PL enhancement is well evidenced at the lowest implantation energy (1 MeV), but at higher energies, a decrease in intensity (2 MeV) and a quenching (3 MeV) are observed. [http://dx.doi.org/10.1063/1.3701696]

I. INTRODUCTION

Although silicon is the most important semiconductor in the microelectronic and photovoltaic industries, for a long time it has not been considered to be suitable for optoelectronic applications because of the indirect nature of its band gap. However, when silicon is in the form of low dimensional structures such as silicon quantum dots (Si QDs), porous silicon or silicon superlattice due to the quantum confinement effect, its optical and electrical properties are quite different from those of bulk silicon. The main advantages of using light emitters based on silicon as Si QDs is that the emission energy and intensity can be controlled by the size, structure and density, and that those systems can be fabricated with CMOS compatible methods such as ion implantation. During the last decade Si QDs-based devices have been already developed, such as LEDs or nonvolatile memories.[1,2] Observation of intense visible photoluminescence and electroluminescence at room temperature and optical gain in Si QDs indicate their potential for optoelectronic applications;[3–6] however, Si QDs show low internal quantum efficiency and radiative decay rates compared to direct band gap semiconductors, as a consequence of the competition between quasi-direct and indirect recombination. To overcome this limitation, the integration of plasmonic materials in the form of metallic nanoparticles or metallic thin films to the semiconductor containing the Si QDs has been used in the last decade. Furthermore, the plasmonic devices have the potential to revolutionize a variety of research fields ranging from nanophotonics and optoelectronics to nanomedicine.

In recent years, Si QDs[7–11] have been successfully coupled to the high density of optical states at the surface plasmon frequency. Besides, it has been well established that metallic nanoparticles, such as Ag and Au, support surface plasmon resonance (SPR), which can be tuned throughout the UV-vis-near-IR spectrum by controlling their shape, size and their local dielectric environment.[12–15]

There are many ways to fabricate nanocrystalline silicon, such as plasma enhanced chemical vapor deposition (PECVD), remote-PECVD (RPECVD),[4,16,17] magnetron sputtering and ion

[a]Corresponding authors: A. Benami. *E-mail address*: abdou_benami@yahoo.fr; A. López-Suárez. *E-mail address*: chipi72@gmail.com

implantation.[6,18,19] In this work we have used the ion implantation technique to obtain a totally integrated configuration formed by Si QDs and silver nanoparticles (Ag NPs). The great advantage of these optical nanocomposites produced by ion implantation is the total protection from environmental effects, such as oxidation due to the way they were fabricated, which makes the devices chemically stables. Here, we present how the photoluminescence presented by these Si QDs can be enhanced or quenched, depending on the distance between the Si QDs and the Ag NPs depth distributions.

II. EXPERIMENTAL

A high-purity silica glass plate ($20\times20\times1$ mm) with OH content less than 1 ppm and total impurity content less than 20 ppm, was implanted at room temperature with 1.5 MeV Si^{+2} ions at fluence of 1.3×10^{17} ions/cm^2, using the 3 MV Tandem accelerator (NEC 9SDH-2 Pelletron) facility at the Instituto de Física of the Universidad Nacional Autónoma de México (IFUNAM). After implantation, the sample was thermally annealed in a reducing atmosphere ($50\%N_2 + 50\%H_2$) at 1100°C for 60 min in order to nucleate the Si QDs from the supersaturated solution and afterwards it was cut into small regular pieces. It has been observed[18,19] that a thermal process performed in a H_2 atmosphere increases the luminescence yield of the Si QDs by passivating the dangling bonds of the material. Once the crystalline Si QDs have been formed inside the matrix, each silica piece was implanted at room temperature with Ag^{+2} ions at different energies (1, 2 and 3 MeV), in order to vary the distance between the Si QDs and the Ag NPs. After the Ag implantation, the samples were again thermally annealed in a reducing environment ($50\%N_2 + 50\%H_2$) at 600°C for 60 min, in order to form the Ag NPs and to reduce the defects produced during the second implantation. Ag was chosen as the element to create the plasmons because this material exhibits the lowest Ohmic damping as well as narrow and strong resonances in the visible wavelength.

Once the Si QDs and Ag NPs were embedded in the same matrix and the distance between them was determined by the Ag implantation energy, the samples were studied and characterized using different techniques. Monte Carlo simulations were performed with the SRIM program to determine the Gaussian depth distribution of the implanted Ag and Si ions; as well as the Si excess and the Ag concentration.[20] According to SRIM, the projectile range or projected range R_p and the straggling ΔR_p of the implanted Ag were in the range 458-1470 nm and 107-269 nm, respectively, as a function of implantation energies. The Si excess concentration was 4.5% and the peak center was located at a depth of 1640 nm.

Photoluminescence (PL) spectroscopy was performed at room temperature at the Nonlinear Optics Laboratory in IFUNAM. 26 ps pulsed at 240 nm from an EKSPLA combined system (PL2143A + PG401/SH) were used as excitation source. Samples were excited from the opposite side to the implantation (Si QDs side), allowing the rapid comparison between PL from QDs in proximity of Ag NPs at different distances. The PL intensity was collected and focused into an optical fiber of 1 mm, and subsequently detected by an Ocean Optics Dual channel SD2000 spectrometer. The optical absorption of all samples was measured by a UV-visible spectrometer (Cary 5000-Varian) in the range of 190-900 nm range.

Rutherford Backscattering Spectrometry (RBS) was used to determine the fluence and Ag depth profile elemental composition using a 3 MeV $^4He^{2+}$ beam. These measurements were also performed at the 3 MV Tandem accelerator (NEC 9SDH-2 Pelletron) facility at the IFUNAM.

III. RESULTS AND DISCUSSION

Fig. 1 shows the PL spectra measured at room temperature of Si QDs with and without the presence of Ag NPs. The PL emission spectra of the reference sample without metallic NPs, is a typical emission of Si QDs embedded in silica matrix. This red emission is centered at 726 nm and spans a wavelength range from 600 to 850 nm. This wide range is due to inhomogeneous distribution of particle size. Passivation with hydrogen removes the defects formed during the implantation process, resulting in a PL signal only due to a quantum confined effect. An enhancement of the emission light for the sample with Ag NPs, implanted at 1 MeV of energy, is observed in Fig. 1.

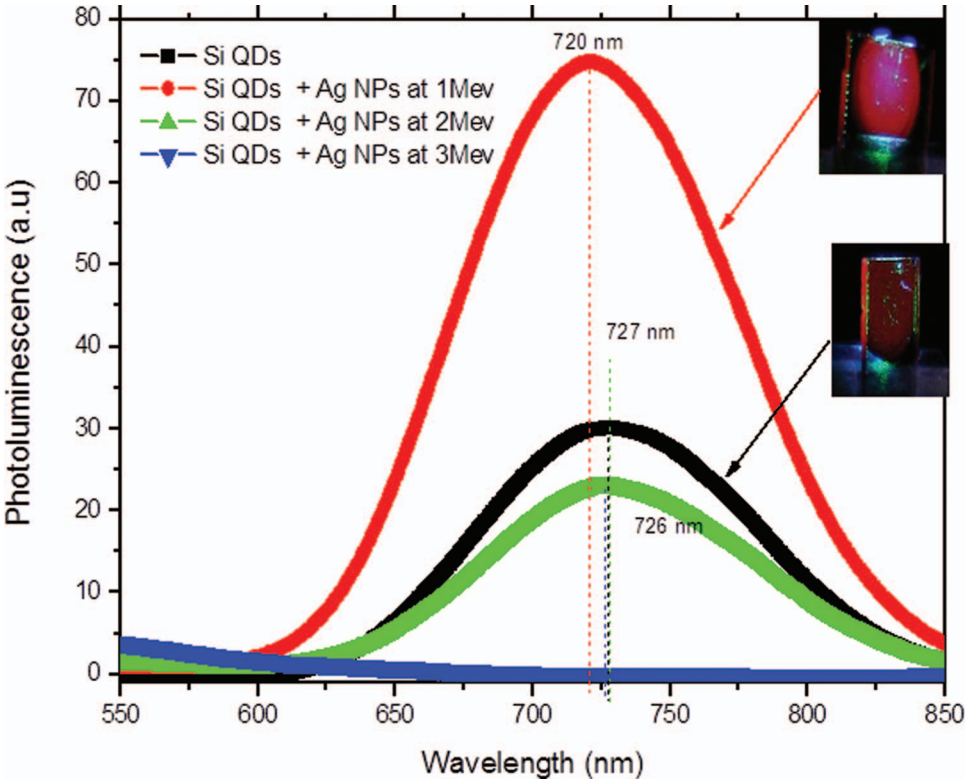

FIG. 1. Photoluminescence spectra at RT of Si QDs in silica with and without the presence of Ag NPs. The insets in the figure show the PL spot with the corresponding emission color visible to the naked eye.

It is clear that the total PL intensity of the system formed by the coupling of the Si QDs and the Ag NPs as a function of the implantation energy is firstly increased, afterwards it tends to decrease and finally it is completely quenched as a function of the implantation energy. The sample with the Ag NPs implanted at 1 MeV of energy, shows a slight blue-shift of the PL peak from 726 nm to 720 nm. This blue-shift is attributed to the presence of Ag NPs that change the density states of the Si QDs.[21] The insert of Fig. 1 shows the red color emission of Si QDs with and without the presence of Ag NPs. The strong brightness of the sample implanted at 1 MeV of energy is clearly visible to naked eye.

The PL enhancement factor, defined as the ratio between the integrated PL intensity due to Si QDs coupled to Ag NPs and the integrated PL intensity of the sample containing only Si QDs, was calculated and reported as a function of the implantation energy in Fig. 2. Here we can distinguish between two processes, one is the enhancement and the other one is the quenching of the PL. As the Ag implantation energy increases,the Si QDs and the Ag NPs distributions get closer, and the PL behavior changes from enhancement to quenching. The observed enhancement factor of 2.5 in the sample containing the Ag NPs implanted at 1 MeV of energy can be clearly assigned to the presence of the metallic nanoparticles.

According to Delerue *et al.*,[22] the size dependent band gap of silicon nanocrystals based on the PL result can be given by

$$E_g = E_b + 3.73/d^{1.39}, \quad (1)$$

where d (nm) is the nanocrystal diameter and E_b =1.12 eV is the band gap of bulk crystal silicon. According to this equation and taking the Si QDs band gap from the PL measurements as E_g = 1.71 eV, the calculated mean diameter of the Si QDs is about 3.7 nm.

An indirect and no destructive way to confirm the formation of Si QDs and Ag NPs is the optical absorption. The absorption edge found at 250 nm (Fig. 3) in the sample without Ag NPs is

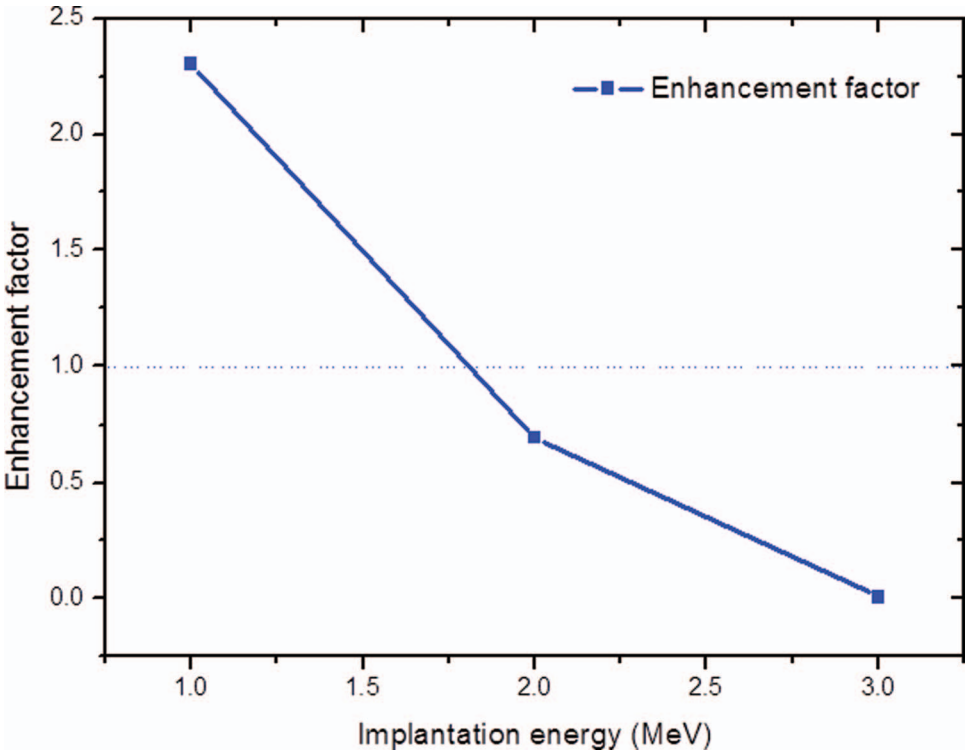

FIG. 2. PL enhancement factor as a function of the implantation energy of Ag ions.

due to the Si QDs embedded in the silica matrix. The absence of defects such as E′ and B_2 indicate that they were eliminated by the hydrogen atoms passivation during the annealing treatment at high temperature. The absorption spectra of each sample containing Ag NPs show a SPR band in the range of 387-391 nm. The presence of these absorbing bands indicates the formation of Ag NPs. According to the narrow absorption peak and the short wavelengths of the plasmon resonance, we can infer that the Ag NPs are small. Assuming the free particle behavior for conduction electrons in Ag NPs, the average diameter of spherical metallic particles, when their size is compared with the wavelength of light, was calculated with the equation

$$\langle D \rangle = \hbar V_F / \Delta E, \tag{2}$$

where V_F=1.4 x 10^6 ms^{-1} is the Fermi velocity of the electrons in the Ag bulk, $\hbar$ is the reduced Planck's constant and ΔE is the full width at half maximum (FWHM) of the absorption band due to the plasmon resonance in small metal particles.[23–25] According to Eq. (2), the mean size of the Ag NPs was 3.11 nm, 3.42 nm and 3.38 nm for the samples implanted at 1 MeV, 2 MeV and 3 MeV, respectively. From our previous works[25,26] in the case of low fluences of Ag ions, i.e. when smaller Ag NPs are formed, no plasmon absorption band was observed, and the samples must then exhibit an absorption band in the UV region between 200 nm and 300 nm (centered around 250 nm), which corresponds to the interband transitions in Ag NPs smaller in size than 2 nm.[27] However, this band does not appear in this work due to the strong absorption related to the presence of the Si QDs in this region and the small amount of Ag NPs.

The blue shift of the surface plasmon of the Ag NPs as a function of implantation energy (Fig. 4) can be attributed to the electron density on their surface, their irregular shape and size and to a change in the refractive index of the matrix.[28,29] Theoretical and experimental results show the linear dependence between position of the peak of the plasmon resonance and the refractive index of the medium.[30,31] The index of refraction of the samples was determined by the m-line prism coupling technique using a He-Ne laser operating at 632.8 nm (1.95 eV). The setup of m-line technique is described elsewhere.[32,33] As the implantation energy of the Ag ions changed from 1 MeV to

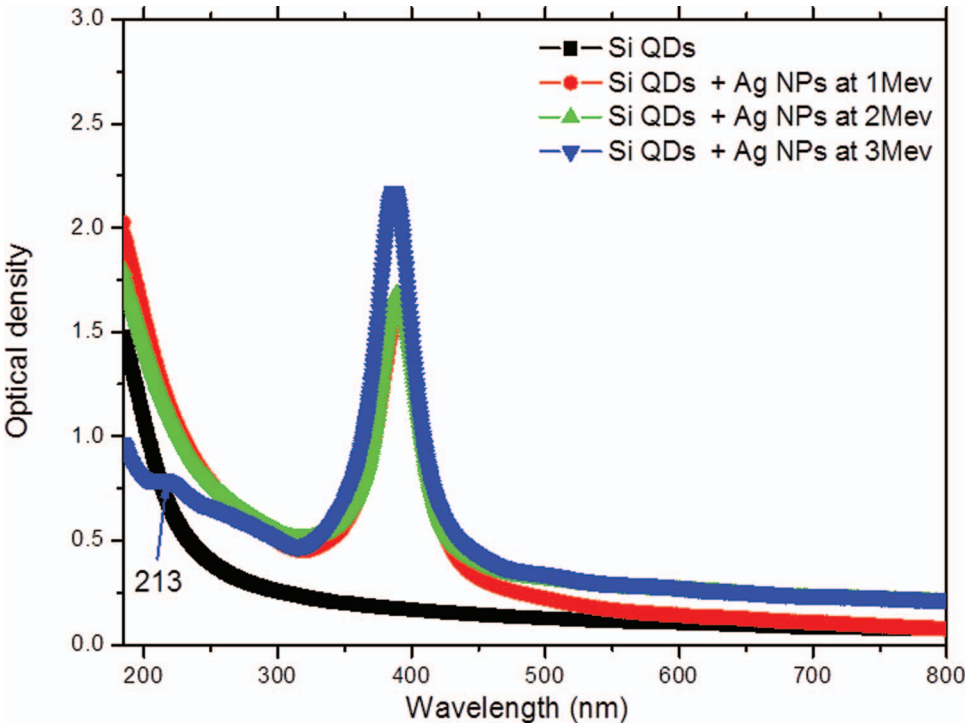

FIG. 3. Optical density of Si QDs samples with and without the presence of Ag NPs.

3 MeV, the refractive index obtained by m-line technique varied between 1.65 and 1.45, which is in reasonable agreement with the shift of the surface plasmon resonance peak.

In order to determine the Ag depth profile as well as the elemental concentration, the RBS spectra were simulated using the SIMNRA code.[34] Fig. 5 shows the 3 MeV $^4He^{+2}$ experimental and simulated RBS spectra of the 1 MeV Ag implanted sample after being annealed in a reducing atmosphere at 600°C. The energy RBS signal of the $^4He^{+2}$ ions backscattered by the Ag atoms can be observed in the 2235-2577 keV energy range, with a maximum at 2378 keV. For comparison, we can mention that the energy of the $^4He^{+2}$ ions backscattered by Ag atoms at the surface of the sample would correspond to 2590 keV, indicating that the Ag NPs are really deep embedded in the silica matrix. As the RBS technique does not allow distinguishing an element from two different sources, the silicon signal due to the Si QDs is veiled by the silicon signal due to the matrix. Fig. 6 shows the 3 MeV $^4He^{+2}$ RBS experimental spectra of the samples containing Si QDs and Ag NPs for the three Ag implantation energies. Fig. 7 shows the Ag concentration depth profile for the three samples containing Si QDs and Ag NPs. Although the Ag distributions are not Gaussians, their peaks' centers match with the ones of the Ag ion range distribution calculated with SRIM. The migration effect to surface of the Ag material in the samples implanted at 2 and 3 MeV showed in Fig. 6, can also be observed in Fig. 7, where the depth profile of the samples are shown. The SIMNRA code also allows the determination of the Ag fluence of the three samples implanted with Ag at 1, 2 and 3 MeV, whose results are 4.44×10^{16} Ag/cm^2, 3.00×10^{16} Ag/cm^2 and 4.24×10^{16} Ag/cm^2, respectively.

The optical properties of metal nanoparticles in the visible region are dominated by the SPR absorption band caused by the collective oscillation of free electrons in response to the electrical field of the excitation light. In addition, as Ag exhibits lower losses in the visible, Ag NPs have an advantage over other metal nanoparticles (i.e., Au and Cu), since the interband transition energy of the Ag in the ultraviolet region is far from the surface plasmon resonance energy. So, in the case of the Ag NPs system we can investigate the optical effects caused exclusively by the interband transition contribution. This effect has not been studied as much as the SPR, so in this work we take

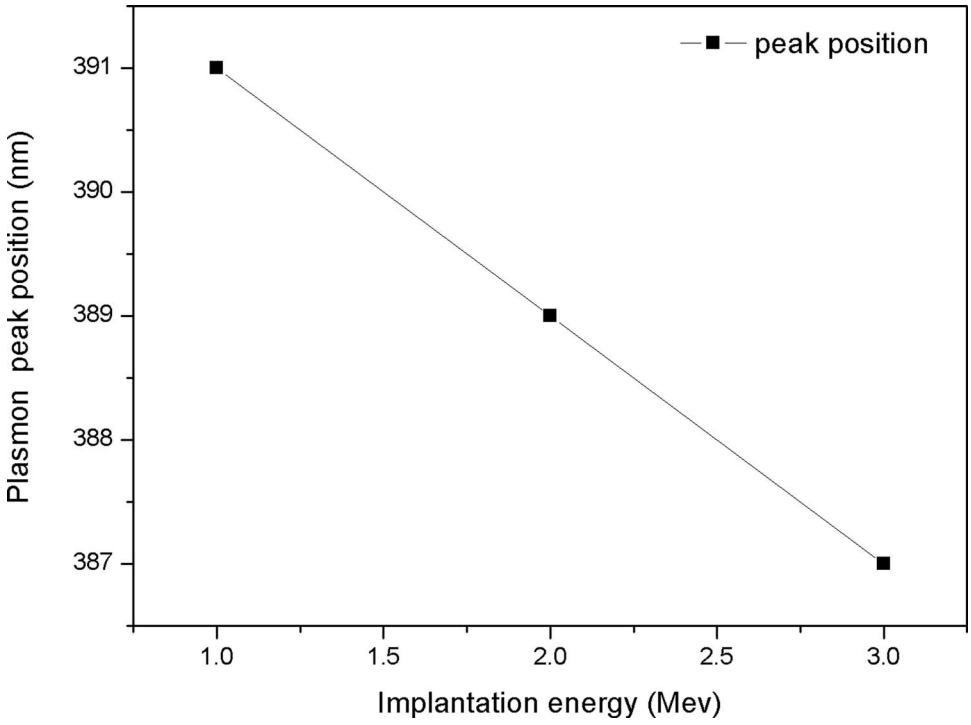

FIG. 4. Position of the SPR peak as a function of the Ag implantation energy.

advantage of the interband transitions in order to improve the optical properties of Si QDs, specially the PL emission.

There are a number of reports that show a relatively strong PL in metal nanostructures.[35,36] When the photoexcitation wavelength is located into the intraband region, or within the same electronic energy band, the luminescence in metal nanostructures is weak. Otherwise if the excitation is located into the interband region, especially when short wavelength light is used, for instance in the UV range, strong photoemission is possible. However, PL from metals even exciting interband transitions is often weaker than in semiconductors due to the high density of states that they present. The origin of the strong PL arising from metal nanoparticles is not always clear, but it could be viewed as an excitation of electrons from occupied *d* bands into states above the Fermi level. Subsequent electron-phonon and hole-phonon scattering processes lead to energy loss and finally to PL recombination of an electron from an occupied *sp* band with a hole.[37]

If we take into account the short wavelength of excitation (240 nm) used in this work, and that the peak of the luminescence spectrum of the metal nanoparticles is centered around the interband absorption edge,[38–40] we can propose two mechanisms to explain the increase in PL of Si QDs near the Ag NPs. The first mechanism is related to the enhancement of the excitation through the emission of Ag NPs centered around 250 nm, that could increase the creation of electron-hole pairs in the Si QDs and then their PL. The second mechanism is related to the enhancement of the quantum efficiency of the Si QDs by coupling to the plasmon modes of the Ag NPs. Nevertheless our Ag NPs are very small, and the excitation wavelength is at 240 nm, far from the Ag NPs SPR, the results suggest that the Si QDs emission interact with the Ag NPs and excite plasmon modes, detecting in the far field region the superposition of both excitations.

The decrease of the PL in the case of the sample implanted at energy of 2 MeV could be attributed to the partial overlapping of the Gaussian tails of the Si QDs and the Ag NPs distributions. This overlapping could decrease the quantity of luminescent centers, diminishing therefore the intensity of the PL intensity. The quenching of the PL signal at all wavelengths observed for the highest Ag implantation energy can be explained as follows: The Ag ions implanted at 3 MeV of energy (which show a nearly Gaussian distribution as the RBS results indicate) have reached the region where the

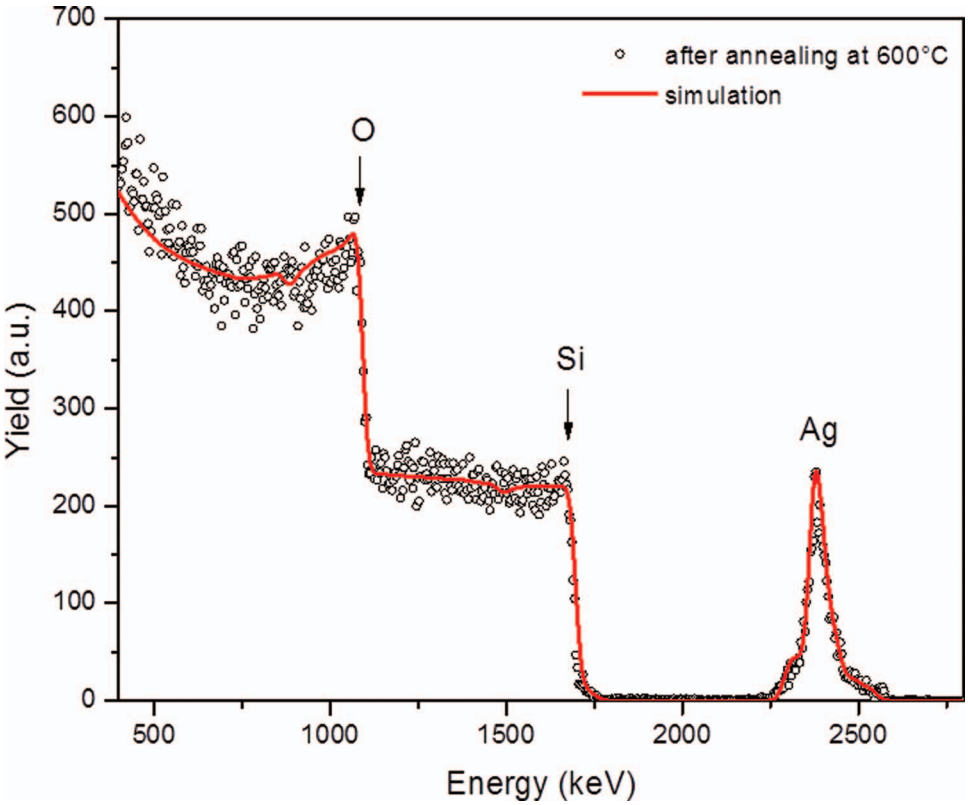

FIG. 5. RBS experimental spectrum of the sample implanted with Ag ions at 1 MeV after annealing at 600°C (dots). The elements that compose the silica substrate (Si and O) can be observed as well as the Ag peak that corresponds to the Ag distribution in the sample. The line that goes over the experimental data corresponds to the SIMNRA simulation of the RBS spectrum.

Si ions have been implanted (see Fig. 8). The quasi total overlapping of the Si QDs and the Ag NPs in Fig. 8 left the Si QDs totally inactive. As expected, this behavior can be explained as the Ag implantation energy is high enough to disintegrate or dissociate the majority of the Si QDs already formed. This fact was confirmed with the UV-Vis results (Fig. 3), and is shown as the lack of the absorption edge relative to the Si QDs. Furthermore, the defects formed during the implantation of Ag ions were partially passivated, when the sample was annealed in hydrogen atmosphere, but also it possible that the presence of these defects rendered the QDs optically inactive, as Pacifici *et al.* previously demonstrated.[41]

A second hypothesis can also explain the quenching of the PL signal. After Ag implantation at 3 MeV, the Si QDs distribution got very closed to the Ag ions. After the annealing at 600°C to nucleate the Ag NPs, a possible Ag-Si alloying can occur, leaving the Si QDs inactive. A 1100°C annealing temperature should be necessary in order to recrystallize the Si QDs, but at this temperature the disintegration of Ag NPs and Ag out diffusion process were previously observed.[42]

IV. CONCLUSION

We have demonstrated the enhancement and quenching of the PL intensity of Si QDs in the vicinity of Ag NPs in a totally integrated configuration. The behavior of the PL emission depends on the Ag implantation energy, which is related to the distance between the Ag NPs and the Si QDs emitters. We propose two mechanisms to explain the origin of the PL enhancement, which differs from the ones based on the coupling between Si QDs emitter and SPR, since the energy of excitation is far from the Ag NPs SPR. Further experiments are required in order to measure the PL lifetime and get a better characterization of the emission enhancement of Si QDs near to the Ag NPs. We

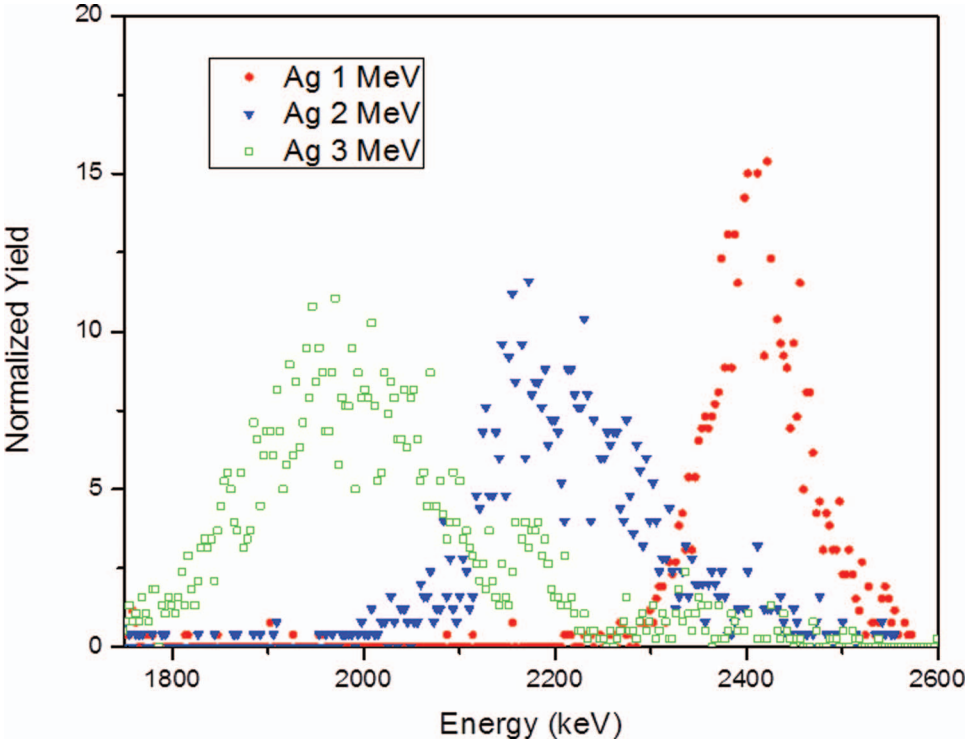

FIG. 6. Detail of the RBS spectra around the Ag signal for the samples implanted with 1, 2 and 3 MeV Ag ions, after annealing at 600°C.

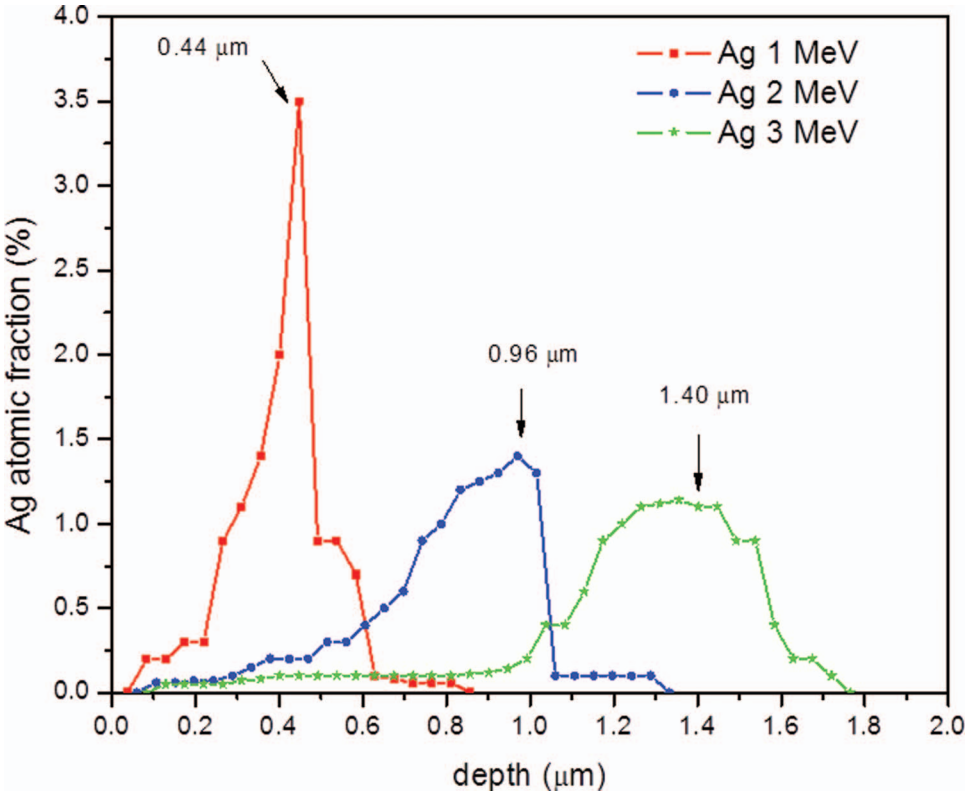

FIG. 7. Ag concentration depth profile for the three samples containing Si QDs and Ag NPs.

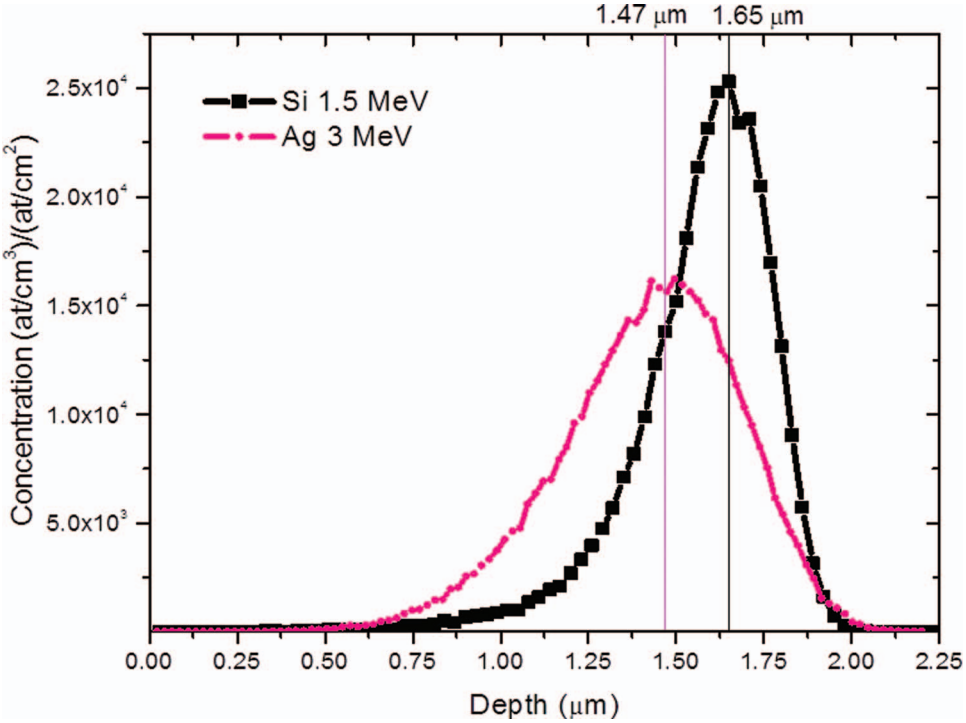

FIG. 8. Numerical Montecarlo simulation of the concentration depth profile for the Si and Ag ions implanted at 1.5 and 3 MeV, respectively.

believe that our integrated device will compete with direct band gap light emitters and that it will possibly be important for the developing of optoelectronic devices based on silicon.

ACKNOWLEDGMENTS

The authors wish to acknowledge the technical assistance of K. López, J.G. Morales and F. J. Jaimes. The support of DGAPA-PAPIIT projects under contracts IN100510-3, IN108412-3 and IN108518 and CONACYT projects under contracts 99224, 102937 and 80019 are also acknowledged.

[1] J. Valenta, N. Lalic, and J. Linnros, Appl. Phys. Lett. **84**, 1459 (2004).
[2] R. J. Walters, P. G. Kik, J. D. Casperson, H. A. Atwater, R. Lindstedt, M. Giorgi, and G. Bourianoff, Appl. Phys. Lett. **85**, 2622 (2004).
[3] L. T. Canham, Appl. Phys. Lett. **57**, 1046 (1990).
[4] A. Benami, G. Santana, A. Ortiz, A. Ponce, D. Romeu, J. Aguilar-Hernández, G. Contreras-Puente, and J. C. Alonso, Nanotechnology **18**, 155704 (2007).
[5] J. C. Alonso, F. A. Pulgarín, B. M. Monroy, A. Benami, M. Bizarro, and A. Ortiz, Thin Solid Films **518**, 3891 (2010).
[6] L. Pavesi, L. Dal Negro, C. Mazzoleni, G. Franzò, and F. Priolo, Nature **408**, 440 (2000).
[7] H. Mertens, J. S. Biteen, H. A. Atwater, and A. Polman, Nano Lett. **6**, 2622 (2006).
[8] J. S. Biteen, L. A. Sweatlock, H. Mertens, N. Lewis, A. Polman, and H. A. Atwater, J. Phys. Chem. C **111**, 13372 (2007).
[9] J. S. Biteen, D. Pacifici, N. S. Lewis, and H. A. Atwater, Nano Lett. **5**, 1768 (2005).
[10] K. Okamoto, S. Vyawahare, and A. Scherer, JOSA B **23**, 1674 (2006).
[11] K. Okamoto, I. Niki, A. Shvartser, Y. Narukawa, T. Mukai, and A. Scherer, Nat. Mater. **3**, 601 (2004).
[12] W. Y. Huang, W. Qian, and M. A. El-Sayed, Nano Lett. **4**, 1741 (2004).
[13] Leif J. Sherry, Rongchao Jin, Chad A. Mirkin, George C. Schatz, and Richard P. Van Duyne, Nano Lett. **6**, 2060 (2006).
[14] W. A. Murray, J. R. Suckling, and W. L. Barnes, Nano Lett. **6**, 1772 (2006).
[15] C. L. Nehl, H. Liao, and J. H. Hafner, Nano Lett. **6**, 683 (2006).
[16] G. Santana *et al.*, Appl. Phys. Lett. **88**, 041916 (2006).
[17] A. Ponce, A. Benami, G. Santana, J. C. Alonso, J. Aguilar-Hernández, G. Contreras-Puente, A. Ortiz, D. Romeu, and J. Fandiño, Phys. Status Solidi C **4**, 1458 (2007).

[18] C. Barthou, P. H. Duong, A. Oliver, J. C. Cheang-Wong, L. Rodriguez-Fernandez, A. Crespo-Sosa, T. Itoh, and P. Lavallard, J. Appl. Phys. **93**, 10110 (2003).
[19] S. Godefroo, M. Hayne, M. Jivanescu, A. Stesmans, M. Zacharias, O. I. Lebedev, G. Van Tendeloo, and V. V. Moshchalkov, Nature Nanotechnology **3**, 174 (2008).
[20] J. F. Ziegler, J. Biersack, and U. Littmark, in *The Stopping and Range of Ions in Solids* (SRIM 2008), http://www.srim.org/.
[21] D. M. Schaadt, B. Feng, and E. T. Yu, Appl. Phys. Lett. **86**, 063106 (2005).
[22] C. Delerue, G. Allan, and M. Lannoo, Phys. Rev. B **48**, 11024 (1993).
[23] W. Cai and V. Shalaev, *Optical Metamaterials: Fundamental and Applications* (Springer, New York, 2010).
[24] S. Dhara, Sharat Chandra, P. Magudapathy, S. Kalavathi, B. K. Panigrahi, K. G. M. Nair, V. S. Sastry, C. W. Hsu, C. T. Wu, K. H. Chen, and L. C. Chen, J. Chem. Phys. **121**, 12595 (2004).
[25] J. Roiz, A. Oliver, E. Muñoz, L. Rodríguez-Fernández, J. M. Hernández, and J. C. Cheang-Wong, J. Appl. Phys. **95**, 1783 (2004).
[26] A. Oliver, J. C. Cheang-Wong, J. Roiz, J. M. Hernández, L. Rodríguez-Fernández, A. Crespo-Sosa, and E. Muñoz, Nucl. Instr. Meth. B **191**, 333 (2002).
[27] K. Shao and J. Yao, Mater. Lett. **60**, 3826 (2006).
[28] J. Z. Zhang and C. Noguez, Plasmonics **3**, 127 (2008).
[29] C. N. R. Rao, A. Muller, and A. K. Cheetham, *Nanomaterials Chemistry: Recent Developments* (Wiley-VCH Verlag, Weinheim, 2007) chap 6, p 185.
[30] K. L. Kelly, E. Coronado, L. L. Zhao, and G. C. Schatz, J. Phys. Chem. **B**, 668 (2003).
[31] C. F. Bohren and D. R. Huffman, *Absorption and Scattering of Light by Small Particles.* (Ed. Wiley, New York, 1998).
[32] R. Th. Kersten, Opt. Acta **22**, 503 (1975).
[33] J. Cardin and D. Leduc, Appl. Opt. **47**, 894 (2008).
[34] M. Mayer, SIMNRA 6.0 User's Guide, Technical Report IPP9/113, Max-Planck-Institut für Plasmaphysik, Garching (1997).
[35] L. A. Peyser, A. E. Vinson, A. P. Bartko, and R. M. Dickson, Science **291**, 103 (2001).
[36] M. B. Mohamed, V. Volkov, S. Link, and M. A. El-Sayed, Chem. Phys. Lett. **317**, 517 (2000).
[37] P. Apell, R. Monreal, and S. Lundqvist, Phys Scr **38**, 174 (1988).
[38] S. L. Smitha, K. M. Nissamudeen, D. Philip, and K. G. Gopchandran, Spectrochim. Acta A **71**, 186 (2008).
[39] S. A. Nepijko, D. N. Ievlev, and W. Schulze, Eur. Phys. J. D **24**, 115 (2003).
[40] P. Gangopadhyay, R. Kesavamoorthy, Santanu Bera, P. Magudapathy, K. G. M. Nair, B. K. Panigrahi, and S. V. Narasimhan, Phys. Rev. Lett. **94**, 047403 (2005).
[41] D. Pacifici, E. C. Moreira, G. Franzò, V. Martorino, F. Priolo, and F. Iacona, Phys. Rev. B **65**, 144109 (2002).
[42] J. C. Cheang-Wong, A. Oliver, J. Roiz, L. Rodríguez-Fernández, J. M. Hernández, and A. Crespo-Sosa, Journal of Physics: Condensed Matter **13**, 10207 (2001).